

Role of FDG PET\CT in the solid renal masses

Essay

Submitted for partial fulfillment of Master Degree In Radiodiagnosis

By

Yahya Eltaher Elshaikh

M.B., B.Ch.

Supervisors

Prof. Dr. Hana Hamdy Nassef

Professor of Radiodiagnosis Faculty of Medicine, Ain Shams University

Mohamed Gamal El-Din Omar

Lecturer of Radiodiagnosis
Faculty of Medicine, Ain Shams University

Faculty of Medicine
Ain Shams University
2015



دور التصوير المقطعي بالانبعاث البوزيتروني / التصوير المقطعي في اورام الكلي

دراست

توطئة مقدمة لكلية الطب جامعة عين شمس للحصول على درجة المحتار في الأشعة التشخيصية

مقدمة من الطبيب/ يحيى الطاهر الشيخ بكالوريوس الطب والجراحة

تحتاشراف الأستاذ الدكتور/هني حمدي ناصف

أستاذ الأشعة التشخيصية كلية الطب جامعة عين شمس

الدكتور/محمد جمال الدين عبدالمطلب

مدرس بقسم الأشعة التشخيصية كلية الطب جامعة عين شمس

كلية الطب جامعة عين شمس م ٢٠١٥

LIST OF THE CONTENTS

List of Tables	Ī
List of Figures	<u>II</u>
Introduction	1
Aim of the work	<u>4</u>
Review of Literature	
Anatomy Of The Kidney	<u>5</u>
Pathology of Solid Renal Masses	<u>21</u>
Principles and Technique of FDG PET – CT	<u>40</u>
Manifestations of Solid renal Tumors by PET/CT	<u>77</u>
Illustrative cases	<u>112</u>
Summary & conclusion	<u>129</u>
References	<u>133</u>
Arabic Summary	-

LIST OF TABLES

Table No.	Title	Page No.
(1)	WHO classification of kidney tumors	23
(2)	FDG PET/CT imaging of renal pathologies	80
(3)	TNM Staging System for Renal Cell Carcinoma	87
(4)	Radiological classification of renal angiomyolipoma	100

LIST OF FIGURES

Fig. No.	Title	Page No.
(1)	The organs of the urinary system are the two kidneys, two ureters, urinary bladder, and urethra	5
(2)	Anatomy of the retroperitoneal spaces at the level of the kidneys	7
(3)	The Anterior surfaces of the kidneys, showing the areas related to neighboring viscera	8
(4)	Drawing illustrates structures related to the posterior surface of each kidney	10
(5)	The internal structures of a kidney	13
(6)	The principal arteries and veins of a kidney	14
(7)	A simplified illustration of blood flow from a glomerulus to an efferent glomerular arteriole, to the peritubular capillaries, and to the venous drainage of the kidney	16
(8)	Axial anatomy at the level of L1 showing the kidneys and their relations	17
(9)	CT section at the level of L1 during arterial corticomedullary phase	18
(10)	Contrast enhanced phases of the kidney on MDCT	19
(11)	Macroscopic and microscopic features of clear cell RCC	26
(12)	(A) Macroscopic appearance of papillary RCC. Microscopic appearance of papillary RCC type 1 (B), type 2 (C)	27
(13)	(A) Macroscopic picture of chromophobe RCC. Microscopic appearance of chromophobe RCC, usual type (B), eosinophilic variant (C)	28
(14)	Unclassified renal cell carcinoma (RCC) showing pure (left top) sarcomatoid carcinoma or unrecognizable cell types	30
(15)	Benign renal cell tumors including papillary adenoma (A), oncocytoma (B) gross and (C) microscopic features and metanephric adenoma (D) gross and (E) microscopic features	32

Fig. No.	Title	Page No.
(16)	a) Renal carcinoid tumor. Grossly it forms a circumscribed mass with a yellow cut surface with foci of hemorrhage. (b) Occasionally, it can have a hemorrhagic and friable cut surface. (c) Microscopically it comprises ribbon and trabeculae of uniform	35
(17)	Uptake of FDG. FDG is a glucose analog that is taken up by metabolically active cells	44
(18)	Annihilation reaction. Positrons (β +) released from the nucleus of FDG annihilate with electrons (β -), releasing two coincidence 511-keV photons (γ), which are detected by scintillation crystals (blue rectangles). N neutron, P proton	
(19)	Production of F-18. After acceleration in a cyclotron, negatively charged hydrogen ions	48
(20)	A typical PET/CT scanner	49
(21)	A typical commercial block detector (8 x 8) attached to four square PM tubes (bottom) and a packaged module (top), developed and manufactured by CPS Innovations	50
(22)	Typical scout image obtained during an FDG PET-CT study	56
(23)	Photograph (side view) of a hybrid PET-CT scanner shows the PET (P) and CT (C) components	57
(24)	Typical imaging protocol for combined PET/CT	59
(25)	Display screen of the syngo software platform shows fused PET-CT images in the sagittal, coronal, and axial planes of a patient with recurrent esophageal carcinoma	61
(26)	Normal distribution of FDG	67
(27)	Normal fluorine-18 fluoro-2-deoxy-Dglucose (FDG) excretion	68
(28)	49-year-old woman with a history of abdominal lymphoma who was referred for post-therapy follow-up	69
(29)	Metal ring on left breast of patient (arrow) produces streaking artifacts and high CT numbers	73

Fig. No.	Title	Page No.
(30)	(A) 58-y-old man with colon cancer. Lesion at dome of liver is mislocalized to right lung (arrow) because of respiratory motion. (B) Image without attenuation correction shows that all lesions are confined to liver (C) Curvilinear cold artifact (arrow) is commonly seen on dome of diaphragm/liver or at lung base because of respiration mismatch on PET images with CT attenuation correction	75
(31)	64-year-old man with incidental renal cell carcinoma (<i>arrows</i>) detected on 18F-FDG PET/CT	85
(32)	Fluorine-18 fluoro-2-deoxy-D-glucose (FDG) positron emission tomography (PET)/CT appearances of a renal cell (RCC) carcinoma with high-grade uptake	86
(33)	62-year-old woman with recurrent renal cell carcinoma (papillary cell type)	91
(34)	Maximum intensity projection (MIP) images of a patient with widespread metastatic disease who underwent F18-FDG PET/CT before (1-A1) and after (1-A2) systemic therapy. The study revealed a significant disease progression and no response to therapy	94
(35)	Maximum intensity projection (MIP) images of a patient with widespread metastatic disease who underwent F18-FDG PET/CT before (2-A1) and after (2-A2) systemic therapy with sunitinib. The study revealed uptake reduction in all sites of disease previously detected but showed new lesions at left internal mammary lymph node chain. Axial fused images of the left humerus before (2-B1) and after (2-B2) the treatment revealing partial response	94
(36)	A patient demonstrating long tumor dormancy. 57 y.o. female with mediastinal lymph node metastasis	95
(37)	84-year-old man with incidentally detected oncocytoma (<i>arrow</i>) arising from left kidney	96
(38)	64-year-old man with intensely 18F-FDG-avid transitional cell carcinoma (<i>arrow</i>) in left lower pole calyx (same patient as in Figure 5)	97

Fig. No.	Title	Page No.
(39)	Fluorine-18 fluoro-2-deoxy-D-glucose (FDG) positron emission tomography (PET)/CT appearances of renal lymphoma. Unenhanced CT image (left) demonstrates bilateral perirenal plaque lesions inseparable from the adjacent renal parenchyma (arrows). PET image (centre) and fused PET/CT image (right) clearly demonstrate increased FDG uptake in these lesions (arrows). Perirenal masses are one of the more typical patterns of renal lymphoma which can be easily identified on metabolic imaging, as an intensely FDG avid lesion	106
(40)	Different patterns of renal involvement by non-Hodgkin lymphoma on axial unenhanced CT, 18F-FDG PET, and fused FDG PET/CT images	107
(41)	Fluorine-18 fluoro-2-deoxy-Dglucose (FDG) positron emission tomography (PET)/CT appearances of renal leukemia	108
(42)	53-year-old woman with history of metastatic breast cancer	110
(43)	51-year-old man with history of metastatic non–small cell lung cancer involving brain and right upper lobe	111
(44)	(FDG-PET)/CT appearances of a renal cell (RCC) carcinoma	113
(45)	62-year-old woman with incidental finding of a renal soft tissue mass lesion A–D , Axial (A and B) MRI and PET CT	115
(46)	FDG PET/CT images: the maximum intensity projection (MIP) image	116
(47)	Axial CT scan (left upper) shows retro-caval lymph node (arrow), which is hypermetabolic on PET (right upper).	118
(48)	Axial CT scan (right upper) shows nodule in the left lung apex (arrow), which is hypermetabolic on PET (right upper)	120
(49)	77-year-old woman with benign looking renal soft tissue mass lesion A–D , Axial (A and B) and coronal (C and D) enhanced CT and fused PET/CT images of large enhancing right renal mass (<i>arrows</i>) demonstrating intense 18F-FDG activity	121

Fig. No.	Title	Page No.
(50)	Contrast-enhanced CT image (left) PET image (middle) and PET/CT image (right) demonstrate a heterogeneous attenuation lesion with fat attenuation in the lower pole of the right kidney on CT (arrow) with minimal uptake of FDG on fused PET/CT image	124
(51)	Fluorine-18 fluoro-2-deoxy-D-glucose (FDG) positron emission tomography (PET)/CT appearances of renal angiomyolipoma (AML). Contrast-enhanced CT image (left) and fused PET/CT image (right) demonstrate a heterogeneous attenuation lesion with fat attenuation in the lower pole of the right kidney on CT (arrow) with minimal uptake of FDG on fused PET/CT image (arrow)	125
(52)	Contrast-enhanced CT confirms an enhancing lesion in the left kidney (arrow)	126
(53)	Fluorine-18 fluoro-2-deoxy-Dglucose (FDG) positron emission tomography (PET)/CT appearances of a potential renal metastasis in a native kidney post-renal transplant	127
(54)	CT, PET, and PET CT images demonstrate markedly increased uptake in mass of the left kidney	128

Introduction

Solid renal masses include pseudotumors and renal neoplasms (*Hélénon et al., 2002*).

Malignant renal masses account for 3% of newly diagnosed cancers, and the most common type (90%) is renal cell carcinoma (RCC). Five-year survival rate in renal cancer patients is 68.4% all over the globe. RCC has shown to be resistant to radiation therapy and chemotherapy, therefore radical or partial nephrectomy remains the mainstay of treatment for localized disease. (*Bertagna et al.*, 2013)

Advances in surgical and chemotherapeutic treatment of primary and metastatic renal malignancies have improved patient outcome. Therefore, accurate diagnosis and correct staging of renal malignancies remains the key to the success of appropriate treatment (*Kumar et al.*, 2005)

Since renal malignancies lack efficient serum markers, the diagnosis solely depends on imaging and results of biopsy. While biopsy remains the gold standard, it is an invasive technique. Moreover, cytology obtained from fine-needle aspiration (FNA), which is less invasive, has poorer diagnostic accuracy (*Kumar et al.*, 2005)

Contrast-enhanced CT or MRI is used as a gold standard imaging modalities in the detection and characterization of renal masses (*Aras et al.*, 2013).

Despite the advantages of current imaging modalities in management of renal solid lesions, they have limitations of evaluating malignant lesions as renal cell carcinoma in regard to local spread and distant disease (*Ramdave et al.*, 2001).

Renal masses that are difficult to diagnose by conventional imaging modalities are complicated cystic lesions, benign solid lesions (oncocytoma and angiomyolipoma), metastatic lesions and lesions smaller than 3 cm. FDG-PET imaging might be more useful in this subset of patients than anatomic imaging (*Kumar et al.*, 2005)

The imaging of tumors with FDG is based on the principle that tumor cells have a higher rate of glucose uptake than normal cells, owing to its higher rate of glycolysis and increased expression of glucose transporters (GLUT-1) at its surface. Renal tumors are not exception, as they do have increased glucose metabolism (*Kumar et al.*, 2005)

Hybrid imaging with positron emission tomography (PET)/computed tomography (CT) provides combined anatomical and functional imaging information allowing for biological characterization of morphological abnormalities seen on CT and vice versa (*Powles et al.*, 2007).

It helps to prevent unnecessary biopsies and ensures optimal management of suspicious lesions based on conventional imaging modalities (*Kochhar et al.*, 2010)

Combining tissue characterization and determining the exact localization and the extent of disease has been shown to result in improved sensitivity and specificity of PET/CT imaging (*Powles et al.*, 2007).

PET/CT with 18F-FDG shows metabolically active disease and is widely used for the diagnosis and follow-up of patients with cancer ,PET/CT with 18F-FDG is widely used for evaluating tumor metabolism in patients with cancer at various time points during the course of the disease . (*Zukotynski et al.*, 2012).

From experience of the Johns Hopkins PET Center, where over 2700 studies were performed in a 2- year period, they foresee that the imaging of the abdominal and pelvic cancer in the future will be almost exclusively done by PET/CT (*Schiepers. 2005*).

Aim of the work

To assess the role of FDG PET CT in evaluation of solid renal masses.

Anatomy Of The Kidney

A. Gross Anatomy

The urinary system consists of two kidneys, two ureters, the urinary bladder, and the urethra (**Fig. 1**). Tubules in the kidneys are intertwined with vascular networks of the circulatory system to enable the production of urine (*Yaqoob*, 2009).

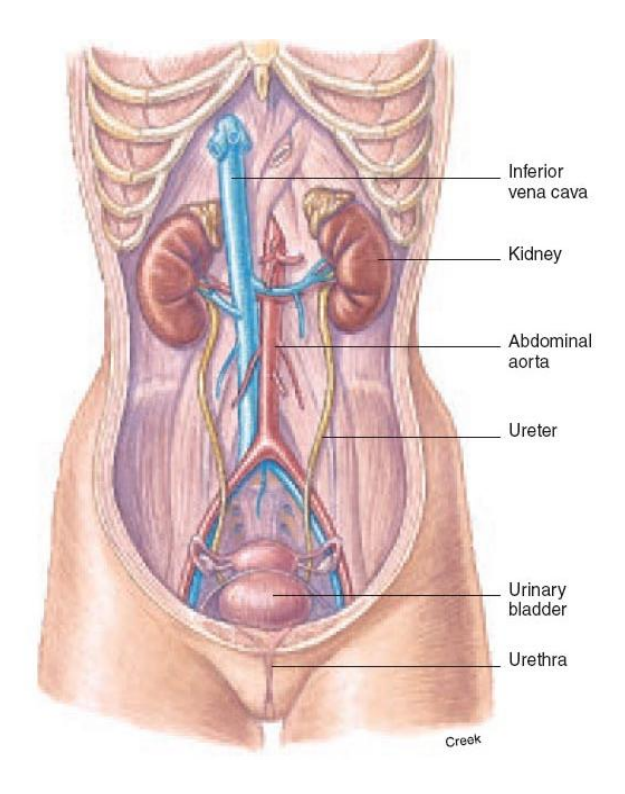


Fig. (1): The organs of the urinary system are the two kidneys, two ureters, urinary bladder, and urethra (Quoted from Yaqoob, 2009).

The kidneys are two bean-shaped organs lying on the retroperitoneal space on either side of the vertebral column in the most posterior part of the abdominal cavity. They lie posterior to the lower portion of the liver on the right and posterior to the lower spleen on the left. The lower ribcage thus forms a protective enclosure for kidneys (*Yaqoob*, *2009*).

The retro peritoneum is divided by facial planes into three compartments: the perirenal, anterior pararenal, and posterior pararenal spaces (anterior and posterior to the renal fascia) (**Fig. 2**) (**Ryan et al., 2004**).

Renal fascia has an anterior leaf "Gerota's fascia" and posterior leaf "Zuckerkandl's fascia". These fascial layers are fused laterally as the lateral conal fascia, which is continuous with the fascia on the deep surface of the transversalis abdominis muscle. Above, the layers blend with the diaphragmatic fascia. Medially, the anterior fascia fuses with the sheaths of the aorta and the inferior vena cava. The posterior fascia fuses with the psoas muscle. The perirenal space contains the kidneys and renal vasculature. Below, the perirenal space is relatively open (*Ryan et al., 2004*).